# Indian Ocean Dipole Response to Global Warming in the CMIP5 Multimodel Ensemble*

XIAO-TONG ZHENG,[+] SHANG-PING XIE,[+,#] YAN DU,[@] LIN LIU,[&] GANG HUANG,[**] AND QINYU LIU[+]

[+] *Key Laboratory of Physical Oceanography, Ministry of Education, and Key Laboratory of Ocean–Atmosphere Interaction and Climate, Ocean University of China, Qingdao, China*

[#] *International Pacific Research Center, and Department of Meteorology, SOEST, University of Hawaii at Manoa, Honolulu, Hawaii, and Scripps Institution of Oceanography, University of California, San Diego, La Jolla, California*

[@] *State Key Laboratory of Tropical Oceanography, SCSIO, Chinese Academy of Sciences, Guangzhou, China*

[&] *Center for Ocean and Climate Research, First Institute of Oceanography, SOA, Qingdao, China*

[**] *LASG, Institute of Atmospheric Physics, Chinese Academy of Sciences, Beijing, China*

(Manuscript received 31 August 2012, in final form 20 February 2013)

ABSTRACT

The response of the Indian Ocean dipole (IOD) mode to global warming is investigated based on simulations from phase 5 of the Coupled Model Intercomparison Project (CMIP5). In response to increased greenhouse gases, an IOD-like warming pattern appears in the equatorial Indian Ocean, with reduced (enhanced) warming in the east (west), an easterly wind trend, and thermocline shoaling in the east. Despite a shoaling thermocline and strengthened thermocline feedback in the eastern equatorial Indian Ocean, the interannual variance of the IOD mode remains largely unchanged in sea surface temperature (SST) as atmospheric feedback and zonal wind variance weaken under global warming. The negative skewness in eastern Indian Ocean SST is reduced as a result of the shoaling thermocline. The change in interannual IOD variance exhibits some variability among models, and this intermodel variability is correlated with the change in thermocline feedback. The results herein illustrate that mean state changes modulate interannual modes, and suggest that recent changes in the IOD mode are likely due to natural variations.

## 1. Introduction

El Niño–Southern Oscillation (ENSO), the dominant mode of ocean–atmosphere interaction in the tropical Pacific, influences tropical and global climate. In recent decades, it is recognized that Indian Ocean (IO) sea surface temperature (SST) anomalies can also impact regional and global climate (Schott et al. 2009). There are two leading modes of Indian Ocean SST variability in observations, referred to as the Indian Ocean basin (IOB) mode (Yang et al. 2007; Du et al. 2009) and Indian Ocean dipole (IOD) mode (Saji et al. 1999; Webster et al. 1999). The basin mode is related to the basinwide warming phenomenon as a remote impact of El Niño—positive SST anomalies develop over the tropical Indian Ocean (TIO) during the boreal winter of the developing year of El Niño, peak in the following spring (Klein et al. 1999; Alexander et al. 2002), and persist through boreal summer (Du et al. 2009, 2013b). On the other hand, the IOD mode features negative (positive) SST anomalies in the southeast equatorial Indian Ocean, and weak positive (negative) anomalies in the west. As a coupled mode, there are easterly (westerly) wind anomalies along the equator over the TIO. The thermocline depth and precipitation fields also show a dipole-like pattern, suggesting that the IOD is an ocean–atmosphere coupled mode. The remote climatic effects of the IOD mode are discussed in Yamagata et al. (2004) and Schott et al. (2009).

Overall the TIO shows a robust warming in the twentieth century due to the greenhouse gases forcing (Du and Xie 2008). The warming is not uniform in space. The warming in the western Indian Ocean is slightly

* International Pacific Research Center Publication Number 954 and School of Ocean and Earth Science and Technology Publication Number 8886.

*Corresponding author address:* Xiao-Tong Zheng, College of Physical and Environmental Oceanography, Ocean University of China, Qingdao 266100, China.
E-mail: zhengxt@ouc.edu.cn

DOI: 10.1175/JCLI-D-12-00638.1

stronger than that in the eastern Indian Ocean. This warming pattern is related to a persistent shoaling of the thermocline in the eastern equatorial Indian Ocean (EIO) over the past 60 years (Alory et al. 2007; Tokinaga et al. 2012). This is consistent with climate projections, where the Walker circulation weakens in response to global warming, and the anomalous easterlies shoal the eastern boundary thermocline (Vecchi et al. 2006; Vecchi and Soden 2007). This long-term thermocline shoaling and the associated subsurface cooling lead to an IOD-like pattern at the surface—reduced (enhanced) SST warming and rainfall over the eastern (western) EIO, with easterly wind change along the equator. Previous studies suggest that the IOD-like pattern, especially the shoaling thermocline in the eastern EIO (EEIO), could strengthen the interannual IOD by enhancing thermocline feedback (Abram et al. 2008). Using coral records and instrumental observations, several studies suggested an IOD intensification over recent decades, with strengthened climate impacts of IOD on East Africa and the Maritime Continent (Abram et al. 2008; Nakamura et al. 2009; Du et al. 2013a). Ihara et al. (2009) investigated the IOD response to global warming based on the coupled general climate models (CGCMs) of phase 3 of the Coupled Model Intercomparison Project (CMIP3), but they did not find an IOD intensification in global warming simulations. So a question arises: Why does the IOD mode of interannual variability not intensify in spite of enhanced thermocline feedback?

To answer this question, Zheng et al. (2010) analyzed the Geophysical Fluid Dynamics Laboratory (GFDL) Climate Model, version 2.1 (CM2.1) CGCM simulation and investigated changes in oceanic and atmospheric processes related to the IOD. They found that while the thermocline shoals and thermocline feedback are enhanced under global warming, atmospheric stratification increases, leading to a weakened atmospheric response to IOD SST anomalies. IOD activity does not change much in a future climate as the result of a balance between the enhanced thermocline and weakened atmospheric feedback. The shoaling thermocline, however, does weaken IOD skewness between opposite phases. While plausible, this hypothesis for IOD change needs to be investigated in other models. The new phase 5 of the Coupled Model Intercomparison Project (CMIP5) offers an opportunity for a multimodel analysis to test the abovementioned results for IOD response to global warming.

The present study examines changes in the mean state of TIO and the interannual IOD mode under global warming by using the CMIP5 multimodel ensemble. The results show that under global warming, changes in both the mean state and IOD mode involve important local air–sea interactions. IOD change is strongly controlled by that of the mean state, indicating that the projection uncertainty for modes of climate variability such as IOD comes from that of the mean state under global warming.

The rest of the paper is organized as follows. Section 2 briefly describes the models and simulations. Section 3 presents the mean state change over TIO under global warming. Section 4 examines the responses of interannual IOD activity and related oceanic and atmospheric feedbacks. The response of IOD skewness to global warming is investigated in section 5. Section 6 is a summary with discussion.

## 2. Models and simulations

This study uses the outputs from the World Climate Research Program (WCRP) CMIP5 multimodel ensemble organized by the Program for Climate Model Diagnosis and Intercomparison (PCMDI) for the Intergovernmental Panel on Climate Change (IPCC) Fifth Assessment Report (AR5). Here we analyze two sets of simulations (Taylor et al. 2012): 106-yr simulations forced by historical greenhouse gases (GHGs), aerosols, and other radiative forcing from 1900 to 2005; and 95-yr projections under the representative concentration pathway (RCP) 8.5 scenario from 2006 to 2100, with the radiative forcing reaching $\sim 8.5\,\mathrm{W\,m^{-2}}$ near 2100 (equivalent to >1370 ppm $CO_2$ in concentration). In this study we use outputs from 17 models, including SST, sea surface height (SSH), surface wind, precipitation, and seawater temperature. In each model, the initial conditions for the RCP8.5 experiment are taken from 1 January 2006 of the historical experiment. So here we combine the two experiments to form a 201-yr-long dataset and examine the TIO mean state change and IOD response to global warming. Table 1 lists the models and provides expansions for all CMIP5 model names. For each model only one member ("r1i1p1") run is used in this study.

This study focuses on the changes of interannual ocean–atmosphere variability over the TIO. To extract interannual signals, we perform a 3-month running mean to suppress intraseasonal variability and remove a 9-yr running mean as decadal and longer variations in each simulation. To examine the oceanic and atmospheric change of IOD events, we use a feedback analysis following Zheng et al. (2010): We measure the strength of thermocline feedback quantitatively using the SST regression upon SSH ($\eta$) in the eastern EIO (10°S–0°, 90°–110°E), $R(T, \eta)$. To measure the strength of atmospheric feedback, we calculate the regression of zonal wind anomalies in the central equatorial Indian Ocean

TABLE 1. The 17 CMIP5 models used in this study.

| Model name | Institute (country) |
|---|---|
| Beijing Climate Center Climate System Model, 1-1 (BCC-CSM1.1) | Beijing Climate Center (BCC), China Meteorological Administration (China) |
| Canadian Earth System Model, version 2 (CanESM2) | Canadian Centre for Climate Modeling and Analysis (Canada) |
| Centre National de Recherches Météorologiques Coupled Global Climate Model, version 5 (CNRM-CM5) | Centre National de Recherches Meteorologiques (France) |
| Commonwealth Scientific and Industrial Research Organisation Mark, version 3.6.0 (CSIRO-Mk3.6.0) | Commonwealth Scientific and Industrial Research Organization in collaboration with the Queensland Climate Change Centre of Excellence (Australia) |
| Geophysical Fluid Dynamics Laboratory Earth Science Model 2G (GFDL-ESM2G) | Geophysical Fluid Dynamics Laboratory (United States) |
| Geophysical Fluid Dynamics Laboratory Earth Science Model 2M (GFDL-ESM2M) | Geophysical Fluid Dynamics Laboratory (United States) |
| Goddard Institute for Space Studies Model E, coupled with Russell ocean model (GISS-E2-R) | NASA Goddard Institute for Space Studies (United States) |
| Hadley Centre Global Environmental Model 2, carbon cycle (HadGEM2-CC) | Met Office Hadley Centre (United Kingdom) |
| Hadley Centre Global Environmental Model 2, Earth System (HadGEM2-ES) | Met Office Hadley Centre (United Kingdom) |
| Institute of Numerical Mathematics Coupled Model, version 4.0 (INM-CM4) | Institute of Numerical Mathematics (Russia) |
| L'Institut Pierre-Simon Laplace Coupled Model, version 5, coupled with NEMO, low resolution (IPSL-CM5A-LR) | Institute Pierre-Simon Laplace (France) |
| L'Institut Pierre-Simon Laplace Coupled Model, version 5, coupled with NEMO, medium resolution (IPSL-CM5A-MR) | Institute Pierre-Simon Laplace (France) |
| Model for Interdisciplinary Research on Climate, version 5 (MIROC5) | University of Tokyo, Atmosphere and Ocean Research Institute, National Institute for Environmental Studies, and Japan Agency for Marine-Earth Science and Technology (Japan) |
| Max Planck Institute Earth System Model, low resolution (MPI-ESM-LR) | Max Planck Institute for Meteorology (Germany) |
| Max Planck Institute Earth System Model, medium resolution (MPI-ESM-MR) | Max Planck Institute for Meteorology (Germany) |
| Meteorological Research Institute Coupled General Circulation Model, version 3 (MRI-CGCM3) | Meteorological Research Institute (Japan) |
| Norwegian Earth System Model, version 1, intermediate resolution (NorESM1-M) | Norwegian Climate Centre (Norway) |

(5°S–5°N, 70°–90°E) upon eastern EIO SST anomalies, $R(U, T)$. To measure the IOD variance, we use the standard deviation of eastern EIO SST anomalies. Here we calculate the regression and standard deviation for the peak phase of IOD, from September to November.

Before the analysis, model simulation skill is examined. We perform an empirical orthogonal function (EOF) analysis of SST anomalies over the TIO (20°S–20°N, 40°–110°E) for 1950–99 for each model. Figure 1 shows SST and surface wind regressions upon the principal component (PC) of the IOD mode in each model and for the ensemble mean. The second EOF mode in most (14 of 17) models features a zonal dipole pattern, while it is the first mode in two models (CSIRO-Mk3.6.0 and INM-CM4) and the third mode in GISS-E2-R. The IOD mode in models explains 16.8% of total variance on average (Fig. 1r), comparable with observations [12%; see Fig. 7 of Deser et al. (2010)]. The spatial pattern of the IOD mode is also comparable with observations in most models, exhibiting an east–west dipole pattern associated with easterly wind anomalies along the equator. The maximum negative SST signal appears along the Java and Sumatra coasts, suggesting that the upwelling effect is important for the IOD development. In several models (e.g., CanESM2, GFDL-ESM2G, IPSL-CM5A-LR, and IPSL-CM5A-MR) the eastern pole of IOD is not located on the eastern EIO region, indicating biases in simulating the upwelling (Fig. 1) in these models.

The models also simulate the phase-locking of IOD. Figure 2 shows ensemble-mean monthly standard deviation of the IOD-related PC, displaying a pronounced seasonality. As in observations, the peak of SST variance appears in September–November (SON). The correlations of the IOD PC with eastern EIO SST and

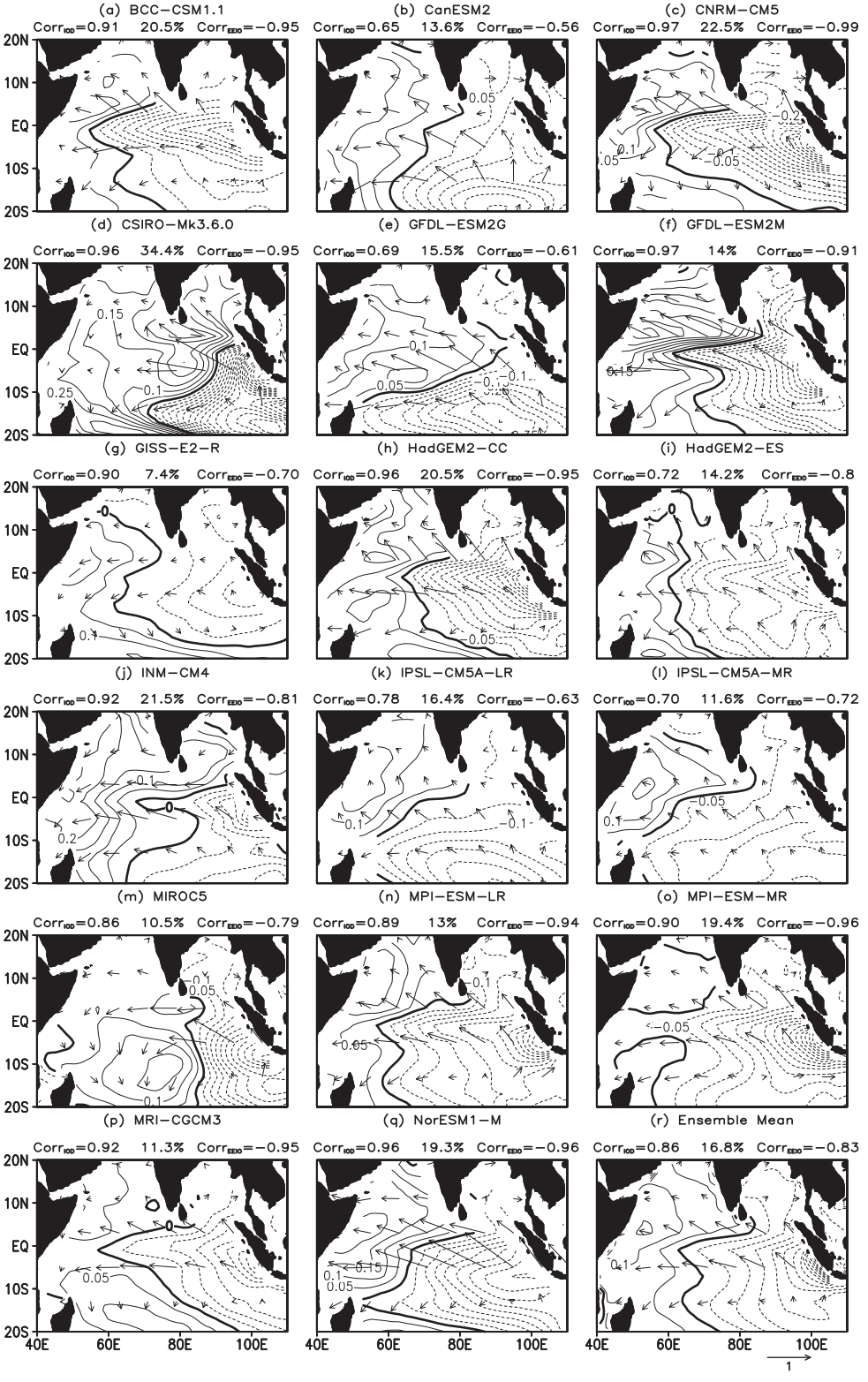


FIG. 1. Regressions of SST (contours at 0.05°C) and surface wind anomalies (vectors) upon the IOD PC in each model and the ensemble mean. The values at the top of each panel are the explained variance (center) and correlations of the IOD PC with the IOD index (left) and eastern EIO SST (right).

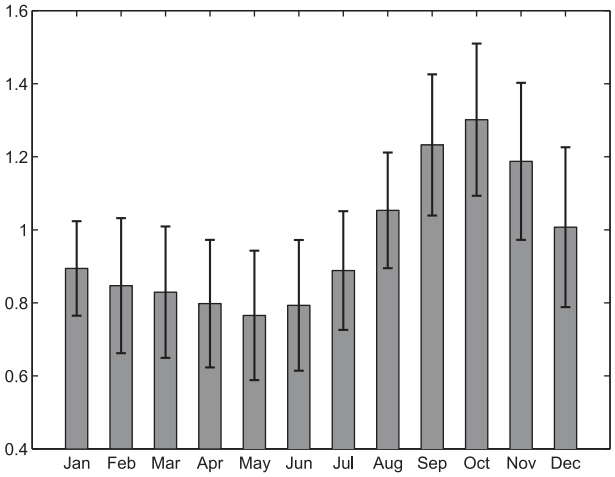


FIG. 2. Ensemble-mean monthly standard deviation of normalized IOD PC. The error bars denote the standard deviation of intermodel variability.

Saji et al.'s (1999) IOD index based on the east–west SST gradient are both highly significant (Fig. 1), and the ensemble mean correlations are −0.83 and 0.86 (Fig. 1r), respectively. Thus we use eastern EIO SST anomalies as the IOD index in this study. Using other indices produces similar results.

## 3. Mean state change

Air–sea interactions for IOD development depend on the mean state of the TIO during boreal summer to fall. To examine the response of IOD to global warming, we first evaluate the mean state change. Figure 3 shows the ensemble mean difference of TIO climatology between the second half of the twenty-first century (2050–99) and twentieth century (1950–99) for boreal summer [June–August (JJA); Fig. 3a] and autumn (SON; Fig. 3b). The ensemble mean SST warming displays an IOD-like pattern: enhanced warming in the northwest IO and reduced warming off the Sumatra and Java coasts. Consistent with previous studies, the precipitation change follows a warmer-get-wetter pattern (Xie et al. 2010; Zheng et al. 2010). Surface wind change is easterly over the EIO, representing a coupled response of the weakened Walker circulation and the SST dipole (Vecchi et al. 2006). The east–west contrast is stronger in boreal autumn, indicating seasonality of the mean state change.

In 4 of 17 models (BCC-CSM1.1, GFDL-ESM2G, INMCM4, and NorESM1-M) the TIO warming does not display a pronounced IOD-like pattern, but the warming pattern is robust in the ensemble mean. Figure 4 shows the ensemble mean indices of the dipole-like SST change, zonal wind change along the equator, and thermocline depth changes in the eastern and western EIO for SON.

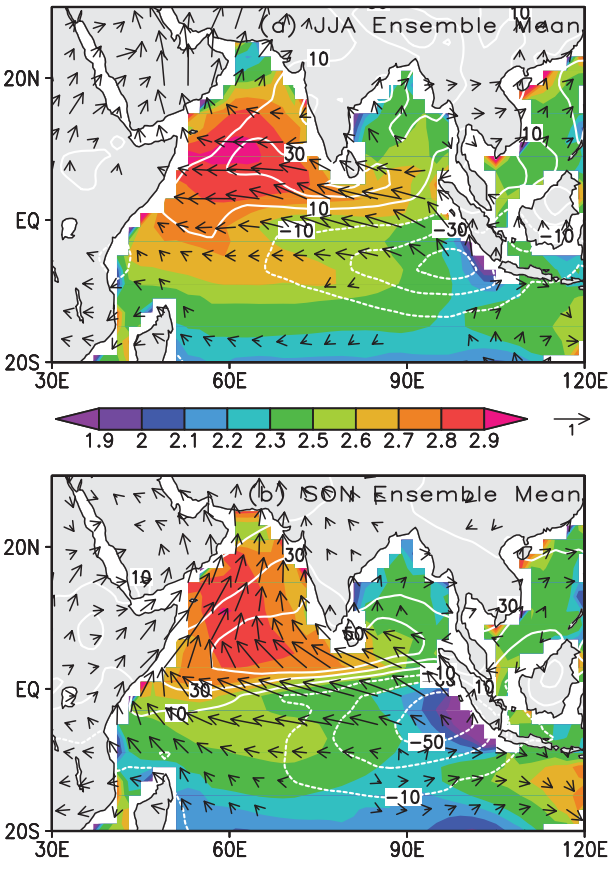


FIG. 3. Ensemble mean of 2050–99 minus 1950–99 differences in SST (color shade, °C), rainfall (contours, mm month$^{-1}$), and surface wind velocity (vectors, m s$^{-1}$) for (a) JJA and (b) SON.

The low-frequency internal variability has been removed by performing the multimodel ensemble mean. The SST zonal gradient over the equatorial IO is largely constant in the twentieth century, and then increases (enhanced warming in the west) gradually by about 0.6°C during the twenty-first century. Meanwhile, the zonal wind over the central EIO shows an easterly change by more than 1 m s$^{-1}$ at the end of the twenty-first century, indicating a weakening of the Walker circulation, a robust response to global warming in CGCM simulations (Vecchi and Soden 2007). In response to the weakened Walker circulation, the subsurface thermal structure also changes, especially in the eastern EIO, where the thermocline shoals. Under global warming, the 20°C isotherm depth deepens and does not represent the thermocline depth well. Therefore we calculate the depth of maximum temperature gradient to represent the dynamical thermocline, following Vecchi and Soden (2007). It is found that the ensemble mean thermocline depth shoals by about 15 m under global warming (Fig. 4c), indicating a close ocean–atmosphere coupling in the IO mean state

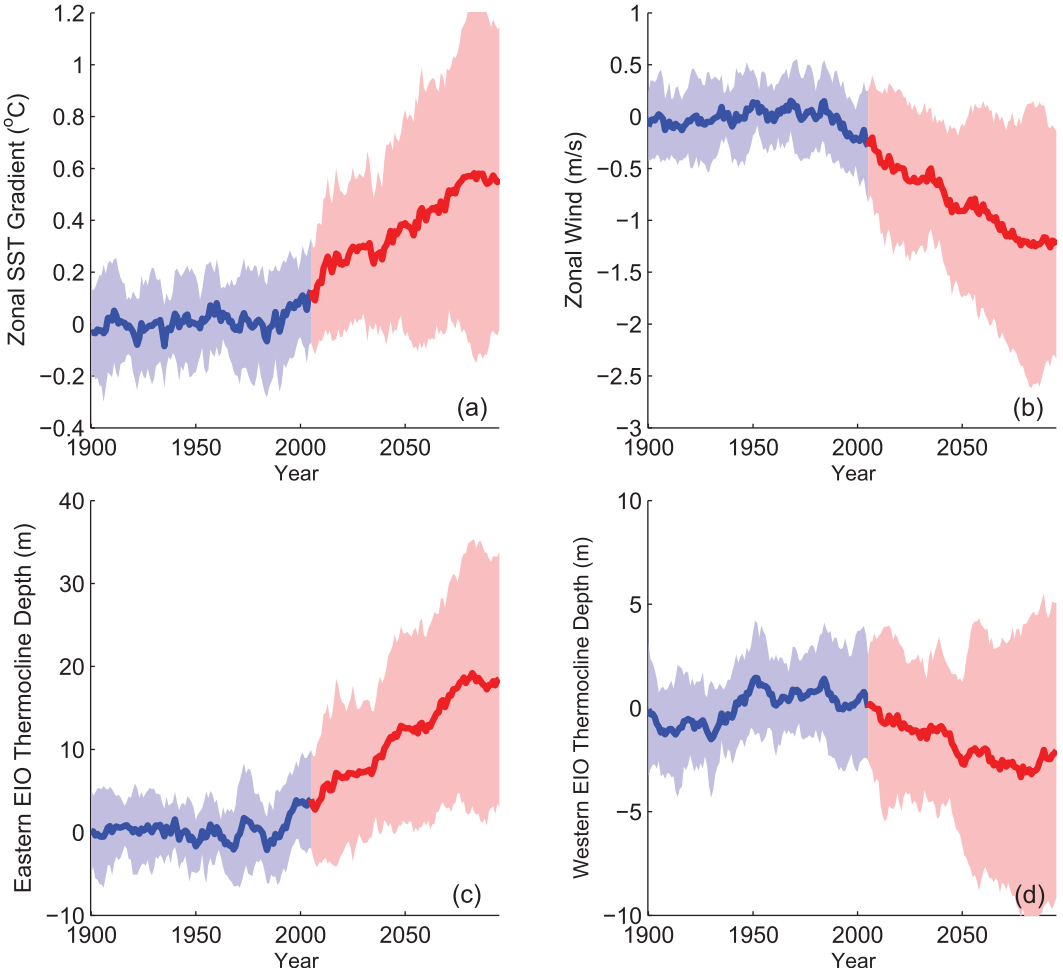


FIG. 4. Ensemble mean of 11-yr running mean time series of (a) IO zonal SST gradient (°C; 50°–70°E, 10°S–10°N minus 90°–110°E, 10°S–0°), (b) equatorial zonal wind ($m\,s^{-1}$; 70°–90°E, 5°S–5°N) and the thermocline depth (m; positive values denote a shoaling thermocline; negative values correspond to a deepening thermocline) in the (c) eastern EIO (90°–110°E, 10°S–0°) and (d) western EIO (50°–70°E, 10°S–10°N) during SON for historical (blue line) and RCP8.5 (red line) simulations referenced to the mean value during 1901–2000. The shading shows one standard deviation of intermodel variability.

change. By contrast, the thermocline in the western EIO deepens slightly (Fig. 4d), consistent with the easterly wind change. It is noticeable that the thermocline shoaling in the eastern EIO is more robust than the dipole-like warming pattern and easterly wind trend. This is likely because the ocean warming is surface intensified, and a thermodynamic shoaling effect is active, in addition to the dynamic adjustment to wind change.

As the IOD-like change strengthens under global warming in ensemble mean indices, the uncertainty of the change also increases due to the diversity of the mean state change among models: At the end of the twenty-first century, the standard deviation of intermodel SST gradient, zonal wind, and eastern EIO thermocline depth changes increase by 0.6°C, $1.2\,m\,s^{-1}$, and 15 m (Fig. 4), respectively. In addition, intermodel variabilities in SST zonal gradients, equatorial zonal wind, and thermocline depth in the eastern EIO are coupled to each other. Figure 5a shows the scatter diagram of intermodel variability in changes of zonal wind in the central EIO and SST gradient for SON. The changes of SST gradient and zonal wind are highly correlated at $r = 0.9$ (the correlation higher than 0.48 is significant at 95% significance level), indicating that if the Walker circulation in a particular model is weakened more (less) than the ensemble mean, the IOD-like SST warming pattern is stronger (weaker) in this model. Furthermore, the changes of thermocline depth and zonal wind also show a significant positive correlation ($r = 0.6$), illustrating the consistency between the

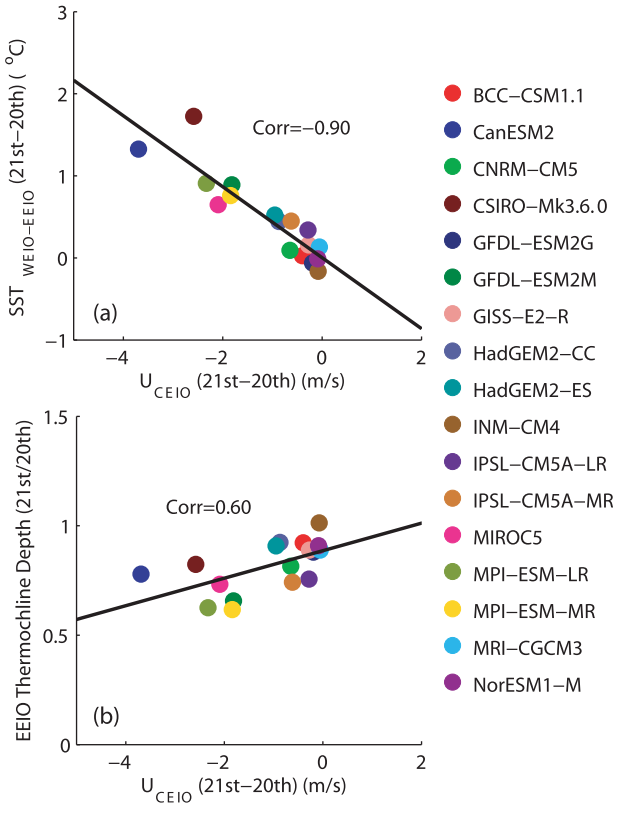


FIG. 5. Scatterplots of central EIO zonal wind change ($m\,s^{-1}$) during SON with (a) zonal SST gradient change (°C), and (b) the ratio of thermocline depth in the eastern EIO between 2050–99 and 1950–99. The solid line denotes the linear regression.

thermocline shoaling in the eastern EIO and weakened Walker circulation under global warming among the models.

Further investigations reveal that the precipitation gradient change across the EIO (west minus east) among the models also shows a correlation with changes in SST gradient, zonal wind, and thermocline depth (not shown). Consistent with the findings of Zheng et al. (2010), the mean state changes among the SST and precipitation east–west gradient, zonal wind, and thermocline depth in the eastern EIO are fully coupled with each other. The diversities of these changes among 17 models, a measure of the uncertainty of model projection, are also highly correlated to each other.

## 4. IOD mode under global warming

This section examines changes in the interannual IOD mode under global warming in relation to the mean state change in the ensemble of 17 CGCMs. We start with IOD variance and then follow with an investigation into thermocline and atmospheric feedbacks.

### *a. Interannual IOD variance*

Since SST variability in the eastern EIO is highly correlated with the IOD index (Saji et al. 1999) based on the west–east SST difference, we represent IOD intensity as the standard deviation of the eastern EIO SST index during SON [$\sigma(T)$]. The IOD intensity change shows some diversity among the models (Figs. 6a,e), but the ensemble mean changes vary little from 0.6°C in 1950–2000 to 0.58°C in 2045–95. IOD strengthens in 7 models and weakens in the other 10 models. The intermodel standard deviation of the change is 0.13°C, indicating uncertainties among the models. Even though the SST activity remains unchanged under global warming in the ensemble mean, the zonal wind variance over the central EIO is obviously reduced (Fig. 6b) in the ensemble mean and most models. The ensemble mean value of interannual standard deviations of zonal wind is 1.5 $m\,s^{-1}$ during 1950–2000 and decreases to 1.2 $m\,s^{-1}$ during 2045–95 by about 20%. Only MIROC5 shows a substantial enhancement of SST and zonal wind variability (Fig. 7), which is due to enhanced thermocline and atmospheric feedbacks (Figs. 8 and 9). Because of the distinct response from other models, we exclude MIROC5 when the ensemble mean standard deviation and atmospheric feedback parameters are calculated. Its inclusion does not change our results qualitatively.

The decrease of zonal wind variance leads to the weakened thermocline variability in the eastern EIO. The interannual variance of the thermocline depth, which is forced by zonal wind anomalies, significantly weakens in a warmer climate (Fig. 6c). The ensemble-mean thermocline depth variance decreases from 16 m in the twentieth century to 11 m in the twenty-first century, a reduction of about 30%. The weakened zonal wind and thermocline variability indicates a decline of the atmospheric component of Bjerknes (1969) feedback in the IOD development. A similar but less significant decrease in variance is also found in eastern EIO precipitation (Fig. 6d), with large diversity among models.

Figure 7b shows the ensemble mean change of the thermal structure in the eastern EIO under global warming. The thermocline in the eastern EIO, tracking the maximum interannual temperature variance (shaded in Fig. 7b), shoals from ~85 m in the late twentieth century to ~70 m at the end of the twenty-first century. As the thermocline shoals, the variance of subsurface temperature decreases. This decrease can also be found in the zonal wind (solid line in Fig. 7a, from ~1.5 to ~1.2 $m\,s^{-1}$) and precipitation (dashed line in Fig. 7a, from ~70 to ~62 mm $month^{-1}$).

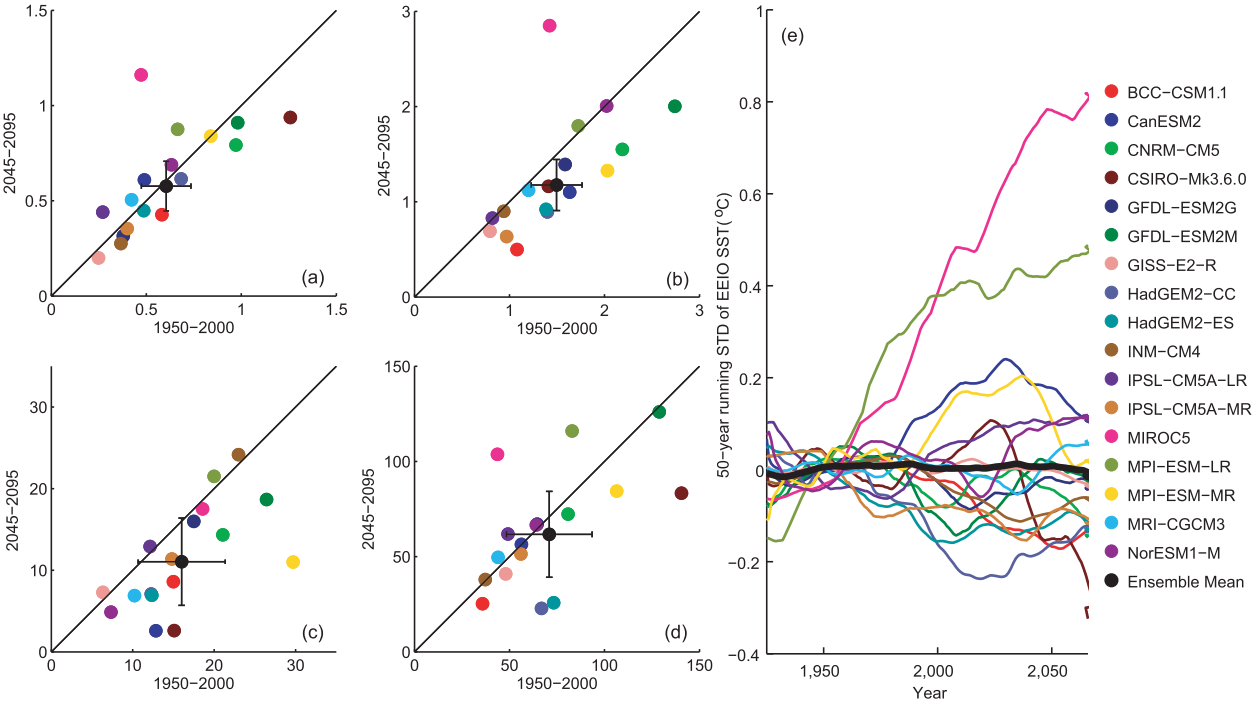


FIG. 6. Scatterplots of standard deviations of (a) eastern EIO SST (°C), (b) central EIO zonal wind (m s$^{-1}$), (c) eastern EIO thermocline depth (m), and (d) eastern EIO precipitation (mm month$^{-1}$) for SON between 1950–2000 and 2045–95. The black dot and error bars denote the ensemble mean and standard deviation of intermodel variability, respectively. MIROC5 is excluded from ensemble mean calculation. (e) The 50-yr running time series of eastern EIO SST (°C) standard deviation for SON in 17 CMIP5 CGCMs referenced to the standard deviation during 1901–2000. The black thick line is multimodel ensemble mean.

### b. *Thermocline feedback*

As the mean thermocline shoals along with the weakened Walker circulation under global warming, the variations of the thermocline depth and upwelling affect SST variability more effectively. Figure 8a shows that the thermocline feedback parameter $R(\text{SST}, \eta)$ increases in most models. The ensemble mean value rises from 11.3°C m$^{-1}$ in 1950–2000 to 13.4°C m$^{-1}$ in 2045–95 by about 18%. In only three models (GFDL-ESM2G, INMCM4, and NorESM1-M) $R(\text{SST}, \eta)$ decreases in a warmer climate. The uncertainty of the change among the models is about 2.2°C m$^{-1}$, close to the ensemble mean change. The time series of $R(\text{SST}, \eta)$ supports the thermocline feedback increase under global warming (Fig. 8c), but the feedback change shows some variations among models and low-frequency natural modulations.

The strengthening of thermocline feedback is due to the thermocline shoaling in the eastern EIO. Figure 8b illustrates the relationship of thermocline feedback change, which is represented by the ratio of $R(\text{SST}, \eta)$ in 2045–95 to 1950–2000, with that of the mean thermocline depth. There is a significant negative correlation ($r = -0.49$): if the thermocline in the eastern EIO shoals more (less) in a coupled model than the ensemble mean, the thermocline feedback is more (less) enhanced. The thermocline feedback change also shows a high correlation ($r = -0.56$) with the zonal wind change in the eastern EIO (not shown). These results suggest that the uncertainty of the IOD oceanic feedback change under global warming is due to the diversity in thermocline change.

### c. *Atmospheric feedbacks*

Despite the shoaling thermocline and strengthened thermocline feedback, the interannual variance decreases under global warming in the thermocline depth (Figs. 6c and 7b), zonal wind, and precipitation (Fig. 7a), indicating a weakened atmosphere response to IOD SST.

Zheng et al. (2010) hypothesized that the atmospheric component of Bjerknes feedback weakens under global warming due to the increased atmospheric dry static stability in the troposphere, the latter a robust feature of atmospheric change (Knutson et al. 1997; Johnson and Xie 2010). We use the zonal wind feedback parameter $R(U, T)$ to evaluate the atmospheric component of Bjerknes feedback. The scatterplot in Fig. 9a compares $R(U, T)$ in the twentieth and twenty-first centuries. A pronounced decline in $R(U, T)$ is found indicating the

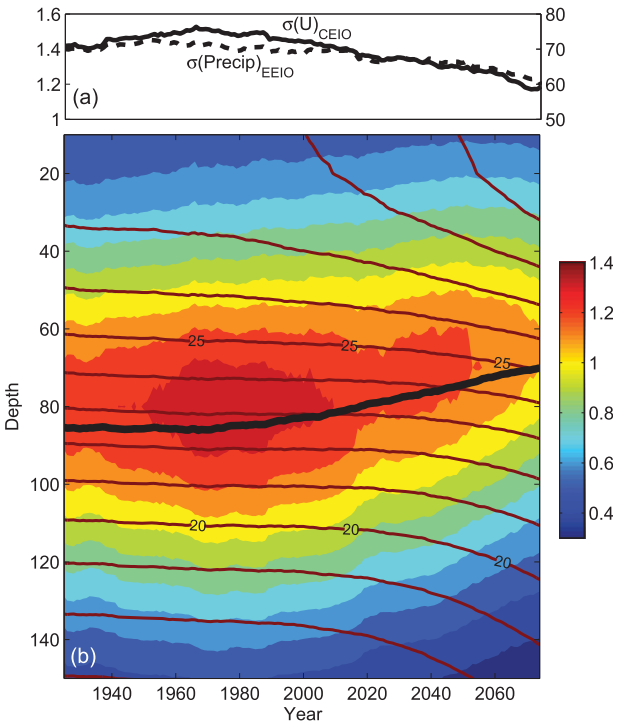


FIG. 7. Ensemble mean standard deviations of interannual variability for SON in 50-yr sliding windows: (a) zonal wind velocity in the central EIO (solid line, $m\,s^{-1}$; left axis) and eastern EIO precipitation (dashed line, mm $month^{-1}$; right axis), and (b) ensemble mean standard deviation of seawater temperature in the eastern EIO (color shading, °C). Also shown in (b) are the thermocline (black solid line) as determined by the maximum gradient in the vertical, and mean seawater temperature (°C) in brown contours.

weakened zonal wind feedback. Only three models (CSIRO-Mk3.6.0, INM-CM4, and MIROC5) simulate a strengthened $R(U, T)$. The ensemble mean value decreases from 2.1 to ~1.7 $m\,s^{-1}$ $°C^{-1}$. The variance of intermodel $R(U, T)$ changes is 0.42 $m\,s^{-1}$ $°C^{-1}$, representing some discrepancy of the atmospheric response among the models. The time series of $R(U, T)$ illustrate the decreasing trend, with some intermodel diversity and low-frequency natural modulations (Fig. 9b).

Furthermore, to investigate the nature of weakened atmospheric IOD feedback, we perform a decomposition of $R(U, T)$ into two parts: the regression of precipitation upon SST anomalies, $R$(Precip, $T$) in the eastern EIO, representing the precipitation response to SST anomalies; and the regression of zonal wind upon precipitation anomalies, $R(U$, Precip), representing the zonal wind response to precipitation anomalies, the latter representing the atmospheric response to a heating source. Both of them are reduced in the twenty-first century but the ensemble mean changes are within the intermodel variance (Fig. 10). Note that $R$(Precip, $T$) weakens in 11 of 17 models with the ensemble mean decreasing from ~98 to ~83 mm $month^{-1}$ $°C^{-1}$; also, $R(U$, Precip) decreases in 13 of 17 models, with the ensemble mean changing from 0.02 to 0.0175 ($m\,s^{-1}$) (mm $month^{-1})^{-1}$. The latter index represents the atmospheric circulation response to anomalous heat source, related to the tropospheric stability. Zheng et al. (2010) emphasized that this term is important for the weakened atmospheric feedback, but the decreased $R$(Precip, $T$) also contributes to the weakened atmospheric feedback. We consider the possible mechanism of the weakened precipitation response. In the eastern EIO region, mean precipitation decreases following the "warmer-get-wetter" mechanism of Xie et al. (2010). The decrease of mean rainfall relative to the current climatology weakens interannual precipitation variability. The abovementioned factors (circulation response to latent heating and precipitation response to SST) both cause the atmospheric feedback to weaken, counteracting the enhanced thermocline feedback.

### d. *Factors for intermodel uncertainty and relationship to ENSO*

The oceanic and atmospheric feedback shows opposing changes and IOD variance changes little in SST. There is a large diversity of $\sigma(T)$ change under global warming among the models (Fig. 6a). So a question arises: Which factor is most important for the intermodel diversity?

To answer this question, we analyze the ratio of $\sigma(T)$ between the twenty-first and twentieth centuries in relation to the ratios of thermocline feedback $R$(SST, $\eta$) and atmospheric feedback $R(U, T)$. Since the $\sigma(T)$ change in MIROC5 is distinct from other models, we exclude MIROC5 from the analysis. There is a significant correlation of the $\sigma(T)$ change with that of $R$(SST, $\eta$) ($r = 0.64$), above 95% significance level based on $t$ test (Fig. 11a). By contrast, there is no correlation between the changes of $\sigma(T)$ and $R(U, T)$ ($r = 0.01$; not shown). These results suggest that even though the weakened atmospheric feedback counters the enhanced thermocline feedback in the ensemble mean, the intermodel variability of $\sigma(T)$ depends on that of $R$(SST, $\eta$).

ENSO is another potential factor for IOD intensity change. We find that there is only a weak correlation between them ($r = 0.22$; Fig. 11b). CMIP5 modes do not show a consistent change in the IOD–ENSO correlation in the presence of global warming (not shown). Therefore, the response of IOD intensity to global warming is mainly controlled by the local oceanic dynamics, the thermocline shoaling in the eastern EIO in particular.

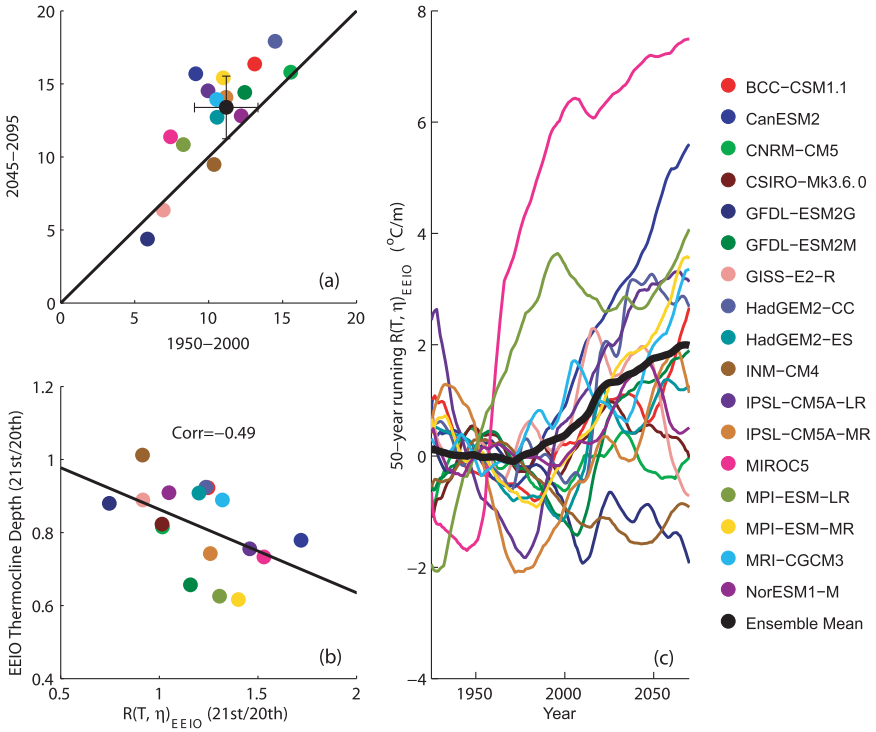


FIG. 8. (a) Scatterplots of $R$(SST, $\eta$) (°C m$^{-1}$) between 1950–2000 and 2045–95. The black dot and error bars denote the ensemble mean and standard deviation of intermodel variability, respectively. (b) Scatterplots of $R$(SST, $\eta$) and thermocline depth ratios between 1950–2000 and 2045–95. The solid line denotes the linear regression. (c) The 50-yr running time series of $R$(SST, $\eta$) (°C m$^{-1}$) for SON in 17 CMIP5 CGCMs referenced to the regression during 1901–2000. The black thick line is multimodel ensemble mean.

## 5. IOD skewness

The asymmetry between positive and negative SST anomalies in the eastern EIO is another important characteristic of IOD (Hong et al. 2008; Ogata et al. 2013). Usually the positive IOD events are much stronger and show a greater climate impact than negative events (Cai et al. 2012). Zheng et al. (2010) suggest a nonlinear thermocline feedback is the reason for the asymmetry of IOD, which is confirmed by observational and modeling studies (Ogata et al. 2013; Cai and Qiu 2013). The asymmetry in eastern EIO SST, measured by skewness, may weaken due to the shoaling thermocline under global warming (Zheng et al. 2010). This section evaluates the IOD skewness in CMIP5 models and investigates its response to global warming.

Figure 12a compares the skewness of SST anomalies in the eastern EIO in the twentieth and twenty-first centuries. Not all the models can capture the observed asymmetry. For current climate (1950–2000), a negative skewness is reproduced in 13 of 17 models with a large diversity among the models. The ensemble mean skewness is −0.6. For a warmer climate (2045–95), the change of skewness tends to be positive in 12 models (except BCC-CSM1.1, GFDL-ESM2G, INM-CM4, IPSL-CM5A-LR, and NorESM1-M). The ensemble mean skewness is −0.36, a decrease of ~40%. This change seems to be insignificant due to a large uncertainty among models.

The intermodel discrepancy of skewness change is related to that of the shoaling thermocline (Fig. 12b). When the thermocline shoaling in the eastern EIO is strong in a model, the skewness change tends to be positive. The correlation of intermodel variability in skewness change with the twenty-first- to twentieth-century thermocline depth ratio is −0.63, indicating the importance of the mean state change.

## 6. Conclusions and discussion

We have investigated the IOD response to global warming and the related mean state change based on historical simulations and future climate projections by 17 CMIP5 models. Under global warming, the ensemble mean thermocline in the eastern EIO shoals by about 15 m. This shoaling thermocline is a result of a weakened Walker circulation and easterly wind change along

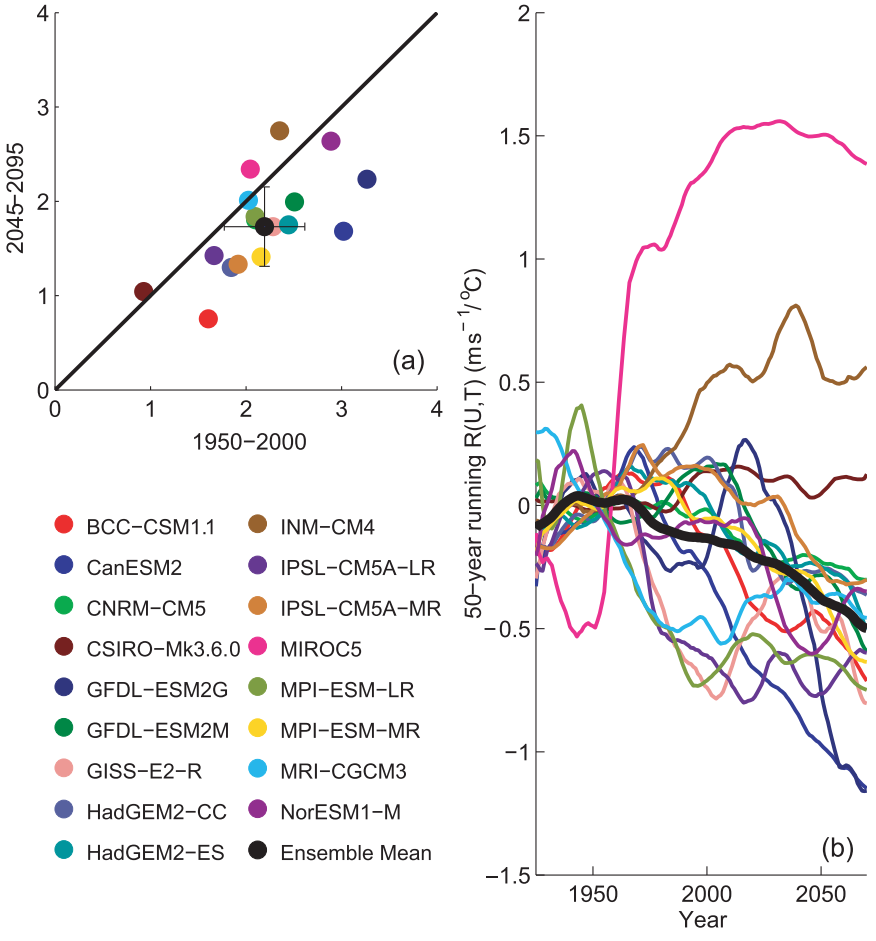


FIG. 9. (a) Scatterplots of $R(U, T)$ ($\mathrm{m\,s^{-1}\,°C^{-1}}$) between 1950–2000 and 2045–95. The black dot and error bars denote the ensemble mean and standard deviation of intermodel variability, respectively. MIROC5 is excluded from ensemble mean calculation. (b) The 50-yr running time series of $R(U, T)$ ($\mathrm{m\,s^{-1}\,°C^{-1}}$) for SON in 17 CMIP5 CGCMs referenced to the regression during 1901–2000. The black thick line is multimodel ensemble mean.

the equator, along with a dipole-like pattern of SST/precipitation change. The intermodel variability in changes of SST, zonal wind, and thermocline depth are highly correlated with each other, indicating the close coupling of ocean–atmosphere fields in TIO.

The mean state change affects the interannual IOD mode, although the ensemble mean IOD variance in SST does not change much under global warming, with some diversity among the models. The shoaling thermocline in the eastern EIO leads to a strengthened thermocline feedback, enabling subsurface temperature anomalies to affect SST more effectively. The strengthening of thermocline feedback, however, does not lead to an intensification of IOD. The atmospheric response weakens, counteracting the stronger thermocline feedback due to a shoaling thermocline. Our decomposition analysis of zonal wind feedback shows that the increased tropospheric stability and reduced interannual variability of precipitation in the eastern EIO are both the reasons for the weakened atmospheric feedback.

Even though the IOD variance change in SST is small in the CMIP5 ensemble mean, the skewness of eastern EIO SST tends to weaken significantly under global warming. The asymmetry of the IOD mode is due to the deep thermocline in the eastern EIO, with a stronger thermocline feedback for cold compared to warm events. By this mechanism, the shoaling of the thermocline in the eastern EIO results in a more linear SST–thermocline relationship and reduces the SST skewness. Indeed, the intermodel variability in skewness change is significantly correlated with that in the thermocline depth, confirming the mean thermocline depth effect on the IOD asymmetry. These results

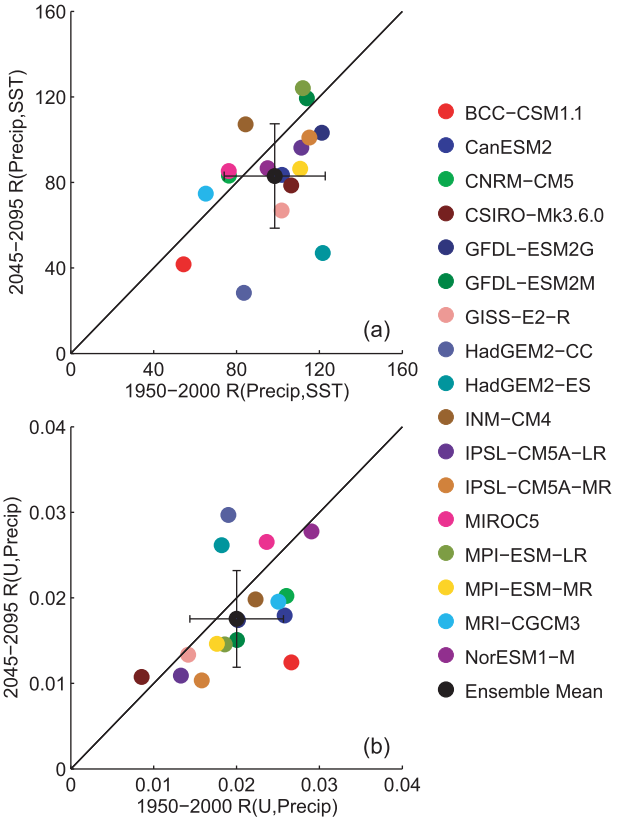


FIG. 10. Scatterplots of (a) $R$(Precip, $T$) (mm month$^{-1}$ °C$^{-1}$) and (b) $R$($U$, Precip) [(m s$^{-1}$)(mm month$^{-1}$)$^{-1}$] between 1950–2000 and 2045–95. The black dot and error bars denote the ensemble mean and standard deviation of intermodel variability, respectively. MIROC5 is excluded from ensemble mean calculation.

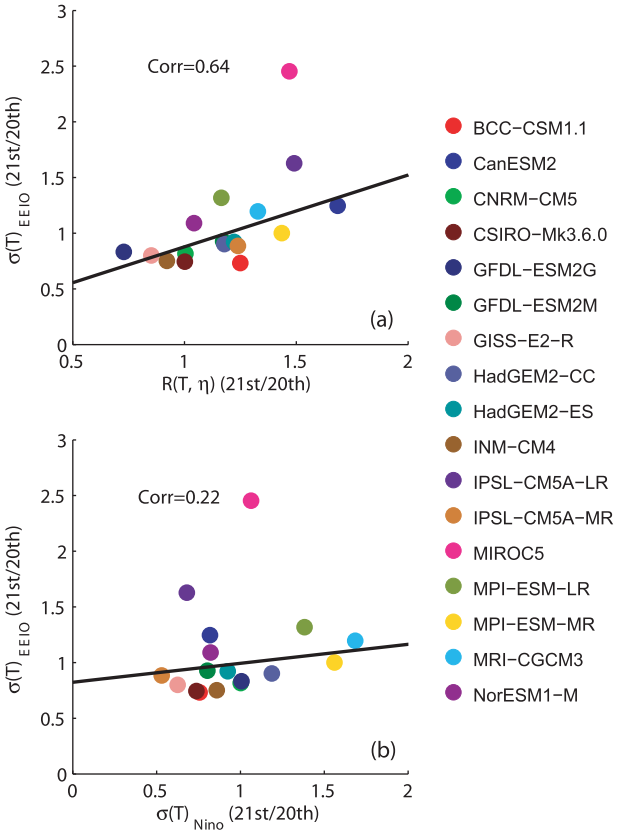


FIG. 11. Scatterplots of the ratios of (a) $R$(SST, $\eta$) (°C m$^{-1}$) and (b) $\sigma(T)_{\text{Niño}}$ (°C) with that of $\sigma(T)_{\text{EEIO}}$ (°C) between the twenty-first and twentieth centuries. The solid line denotes the linear regression. MIROC5 is excluded from correlation calculation.

suggest that the mean state change is very important for the climate mode response to global warming. Since the IOD generates considerable influences on local and remote climate by affecting atmospheric convection, the changes in IOD climatic impacts need to be investigated in future studies.

While the ensemble-mean IOD variance in SST remains unchanged in global warming, there is considerable variability among models in this change (Fig. 6a). The intermodel variability in eastern IO SST variance is only weakly correlated with ENSO amplitude, and much more highly correlated with changes in thermocline feedback (Fig. 11). Thus, the IOD variance change in the future appears to be largely determined by internal ocean–atmospheric feedback within the TIO, in particular the thermocline depth change in the eastern EIO.

We have shown that most CMIP5 models display an IOD-like pattern in the mean state change, including an enhanced (reduced) warming in the west (east), a weakened Walker cell, and shoaling thermocline in the east. Such a pattern of climate change may have emerged from observations (Abram et al. 2008; Du et al. 2013a). Indeed, precipitation over the Maritime Continent has been decreasing (Tokinaga et al. 2012) as projected by models, associated with the Walker circulation slowdown. Conflicting results, however, were obtained from reanalysis (Han et al. 2010), illustrating the difficulty detecting climate change signals amid natural variability from limited observations.

This study focuses on changes of interannual IOD variability under global warming. The tropical Indian Ocean also shows interdecadal variability (Ashok et al. 2004; Annamalai et al. 2005; Schott et al. 2009; Nidheesh et al. 2013). Interdecadal variations influence the IOD mode by modulating the background state (Annamalai et al. 2005; Zheng et al. 2010). Indeed, there are apparent interdecadal variations in eastern EIO SST standard deviation (Fig. 6e), thermocline feedback (Fig. 8c), and atmospheric feedback (Fig. 9b) in CMIP5 models. While the multimodel mean suppresses low-frequency natural modulation, the interference effect by interdecadal

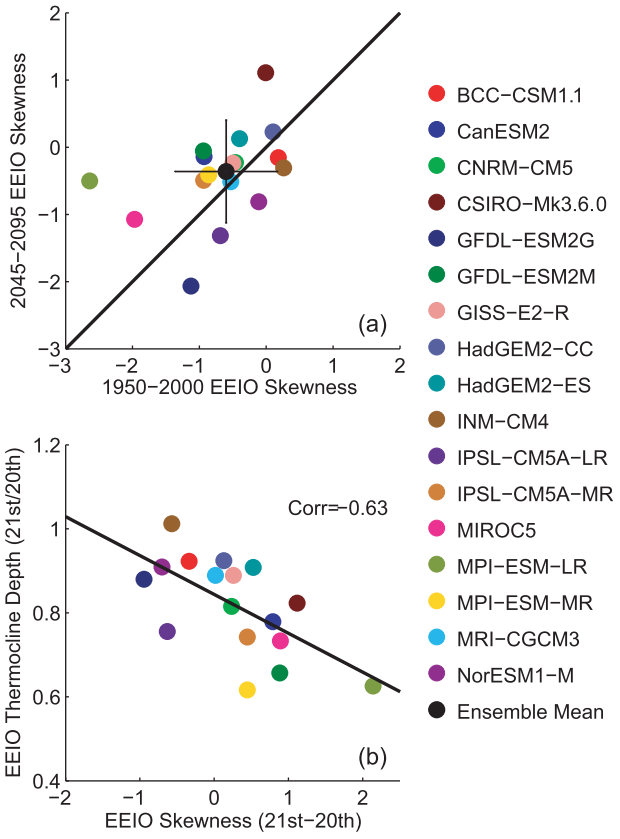


FIG. 12. (a) Scatterplots of eastern EIO SST skewness between 1950–2000 and 2045–95. The black dot and error bars denote the ensemble mean and standard deviation of intermodel variability, respectively. (b) Scatterplots of the change of eastern EIO skewness and the ratio of thermocline depth between the twenty-first and twentieth centuries. The solid line denotes the linear regression. MIROC5 is excluded from ensemble mean correlation calculations.

variations on detecting the IOD response to anthropogenic forcing needs further investigation, especially for individual models.

*Acknowledgments.* We acknowledge the World Climate Research Programme's Working Group on Coupled Modelling, which is responsible for CMIP, and we thank the climate modeling groups for producing and making available their model output. For CMIP the U.S. Department of Energy's Program for Climate Model Diagnosis and Intercomparison provides coordinating support and led development of software infrastructure in partnership with the Global Organization for Earth System Science Portals. We wish to thank L. X. Xu and S. M. Long for data preparation. This work is supported by the National Basic Research Program of China (2012CB955600), the Natural Science Foundation of China (41106010, 41176006, 40921004), the 111 Project (B07036), the Chinese Academy of Sciences (XDA05090400, LTOZZ1202), the Qianren Programs, the U.S. National Science Foundation, and the Japan Agency for Marine-Earth Science and Technology.

## REFERENCES

Abram, N. J., M. K. Gagan, J. E. Cole, W. S. Hantoro, and M. Mudeless, 2008: Recent intensification of tropical climate variability in the Indian Ocean. *Nat. Geosci.,* **1,** 849–853.

Alexander, M. A., I. Bladé, M. Newman, J. R. Lanzante, N.-C. Lau, and J. D. Scott, 2002: The atmospheric bridge: The influence of ENSO teleconnections on air–sea interaction over the global oceans. *J. Climate,* **15,** 2205–2231.

Alory, G., S. Wijffels, and G. Meyers, 2007: Observed temperature trends in the Indian Ocean over 1960–1999 and associated mechanisms. *Geophys. Res. Lett.,* **34,** L02606, doi:10.1029/2006GL028044.

Annamalai, H., J. Potemra, R. Murtugudde, and J. P. McCreary, 2005: Effect of preconditioning on the extreme climate events in the tropical Indian Ocean. *J. Climate,* **18,** 3450–3469.

Ashok, K., W.-L. Chan, T. Motoi, and T. Yamagata, 2004: Decadal variability of the Indian Ocean dipole. *Geophys. Res. Lett.,* **31,** L24207, doi:10.1029/2004GL021345.

Bjerknes, J., 1969: Atmospheric teleconnections from the equatorial Pacific. *Mon. Wea. Rev.,* **97,** 163–172.

Cai, W., and Y. Qiu, 2013: An observation-based assessment of nonlinear feedback processes associated with the Indian Ocean dipole. *J. Climate,* **26,** 2880–2890.

——, P. van Rensch, T. Cowan, and H. H. Hendon, 2012: An asymmetry in the IOD and ENSO teleconnection pathway and its impact on Australian climate. *J. Climate,* **25,** 6318–6329.

Deser, C., M. A. Alexander, S.-P. Xie, and A. S. Phillips, 2010: Sea surface temperature variability: Patterns and mechanisms. *Annu. Rev. Mar. Sci.,* **2,** 115–143, doi:10.1146/annurev-marine-120408-151453.

Du, Y., and S.-P. Xie, 2008: Role of atmospheric adjustments in the tropical Indian Ocean warming during the 20th century in climate models. *Geophys. Res. Lett.,* **35,** L08712, doi:10.1029/2008GL033631.

——, ——, G. Huang, and K. Hu, 2009: Role of air–sea interaction in the long persistence of El Niño–induced North Indian Ocean warming. *J. Climate,* **22,** 2023–2038.

——, W. Cai, and Y. Wu, 2013a: A new type of the Indian Ocean dipole since the mid-1970s. *J. Climate,* **26,** 959–972.

——, S.-P. Xie, Y.-L. Yang, X.-T. Zheng, L. Liu, and G. Huang, 2013b: Indian Ocean variability in the CMIP5 multimodel ensemble: The basin mode. *J. Climate,* in press.

Han, W., and Coauthors, 2010: Patterns of Indian Ocean sea-level change in a warming climate. *Nat. Geosci.,* **3,** 546–550.

Hong, C.-C., T. Li, LinHo, and J.-S. Kug, 2008: Asymmetry of the Indian Ocean dipole. Part I: Observational analysis. *J. Climate,* **21,** 4834–4848.

Ihara, C., Y. Kushnir, M. A. Cane, and V. H. de la Peña, 2009: Climate change over the equatorial Indo-Pacific in global warming. *J. Climate,* **22,** 2678–2693.

Johnson, N. C., and S.-P. Xie, 2010: Changes in the sea surface temperature threshold for tropical convection. *Nat. Geosci.,* **3,** 842–845.

Klein, S. A., B. J. Soden, and N.-C. Lau, 1999: Remote sea surface temperature variations during ENSO: Evidence for a tropical atmospheric bridge. *J. Climate,* **12,** 917–932.

Knutson, T. R., S. Manabe, and D. Gu, 1997: Simulated ENSO in a global coupled ocean–atmosphere model: Multidecadal amplitude modulation and $CO_2$ sensitivity. *J. Climate,* **10,** 138–161.

Nakamura, N., H. Kayanne, H. Iijima, T. R. McClanahan, S. K. Behera, and T. Yamagata, 2009: Mode shift in the Indian Ocean climate under global warming stress. *Geophys. Res. Lett.,* **36,** L23708, doi:10.1029/2009GL040590.

Nidheesh, A. G., M. Lengaigne, J. Vialard, A. S. Unnikrishnan, and H. Dayan, 2013: Decadal and long-term sea level variability in the tropical Indo-Pacific Ocean. *Climate Dyn.,* doi:10.1007/s00382-012-1463-4, in press.

Ogata, T., S.-P. Xie, J. Lan, and X. Zheng, 2013: Importance of ocean dynamics for the skewness of the Indian Ocean dipole mode. *J. Climate,* **26,** 2145–2159.

Saji, N. H., B. N. Goswami, P. N. Vinayachandran, and T. Yamagata, 1999: A dipole mode in the tropical Indian Ocean. *Nature,* **401,** 360–363.

Schott, F. A., S.-P. Xie, and J. P. McCreary, 2009: Indian Ocean circulation and climate variability. *Rev. Geophys.,* **47,** RG1002, doi:10.1029/2007RG000245.

Taylor, K. E., R. J. Stouffer, and G. A. Meehl, 2012: An overview of CMIP5 and the experiment design. *Bull. Amer. Meteor. Soc.,* **93,** 485–498.

Tokinaga, H., S.-P. Xie, A. Timmermann, S. McGregor, T. Ogata, H. Kubota, and Y. M. Okumura, 2012: Regional patterns of tropical Indo-Pacific climate change: Evidence of the Walker circulation weakening. *J. Climate,* **25,** 1689–1710.

Vecchi, G. A., and B. J. Soden, 2007: Global warming and the weakening of the tropical circulation. *J. Climate,* **20,** 4316–4340.

——, ——, A. T. Wittenberg, I. M. Held, A. Leetmaa, and M. J. Harrison, 2006: Weakening of tropical Pacific atmospheric circulation due to anthropogenic forcing. *Nature,* **441,** 73–76.

Webster, P. J., A. Moore, J. Loschnigg, and M. Leban, 1999: Coupled ocean–atmosphere dynamics in the Indian Ocean during 1997–98. *Nature,* **401,** 356–360.

Xie, S.-P., C. Deser, G. A. Vecchi, J. Ma, H. Teng, and A. T. Wittenberg, 2010: Global warming pattern formation: Sea surface temperature and rainfall. *J. Climate,* **23,** 966–986.

Yamagata, T., S. K. Behera, J.-J. Luo, S. Masson, M. Jury, and S. A. Rao, 2004: Coupled ocean–atmosphere variability in the tropical Indian Ocean. *Earth's Climate: The Ocean–Atmosphere Interaction, Geophys. Monogr.,* Vol. 147, Amer. Geophys. Union, 189–212.

Yang, J., Q. Liu, S.-P. Xie, Z. Liu, and L. Wu, 2007: Impact of the Indian Ocean SST basin mode on the Asian summer monsoon. *Geophys. Res. Lett.,* **34,** L02708, doi:10.1029/2006GL028571.

Zheng, X.-T., S.-P. Xie, G. A. Vecchi, Q. Liu, and J. Hafner, 2010: Indian Ocean dipole response to global warming: Analysis of ocean–atmospheric feedbacks in a coupled model. *J. Climate,* **23,** 1240–1253.